Supporting Information

Confined Cavity on a Mass-Producible Wrinkle Film Promotes the Selective CO₂ Reduction

Dr. Kyeong Min Cho,[ab†] Dr. Woo-Bin Jung,[abe†] Dr. Donggyu Kim,[c] Dr. Ju Ye Kim,[ab] Ye Sol Kim,[ab] Geun-Tae Yun,[ab] Prof. Seunghwa Ryu,[c] Dr. Ahmed Al-Saggaf,[d] Dr. Issam Gereige [d] and Prof. Hee-Tae Jung *[ab]

[a]	Dr. K. M. Cho, Dr. W.-B. Jung, Dr. J. Y. Kim, Y. S. Kim, G.-T. Yun, Prof.H.-T. Jung*
	Department of Chemical and Biomolecular Engineering
	Korea Advanced Institute of Science and Technology (KAIST)
	Daejeon 34141, Republic of Korea
	E-mail: heetae@kaist.ac.kr
[b]	Dr. K. M. Cho, Dr. W.-B. Jung, Dr. J. Y. Kim, Y. S. Kim, G.-T. Yun, Prof.H.-T. Jung*
	KAIST Institute of Nanocentury
	Daejeon 34141, Republic of Korea
[c]	Dr. D. Kim, Prof. S. Ryu
	Department of Mechanical Engineering
	Korea Advanced Institute of Science and Technology (KAIST)
	Daejeon 34141, Republic of Korea
[d]	A. Al-Saggaf, I. Gereige
	Research and Development Center
	Saudi Aramco
	Dhahran 31311, Saudi Arabia
[e]	Dr. W.-B. Jung
	School of Engineering and Applied Sciences
	Harvard University
	Cambridge, Massachusetts 02138, USA.
†	These authors contributed equally to this work.

Table of contents:

SEM images of wrinkles with varying thickness and strain

We controlled the morphology of wrinkle films varying with a thickness from 25 nm to 100 nm and a strain from 0.25 to 0.75. The structural parameters of wrinkle films such as wavelength, amplitude, existence of confined cavity was investigated to increase the activity of CO_2RR.
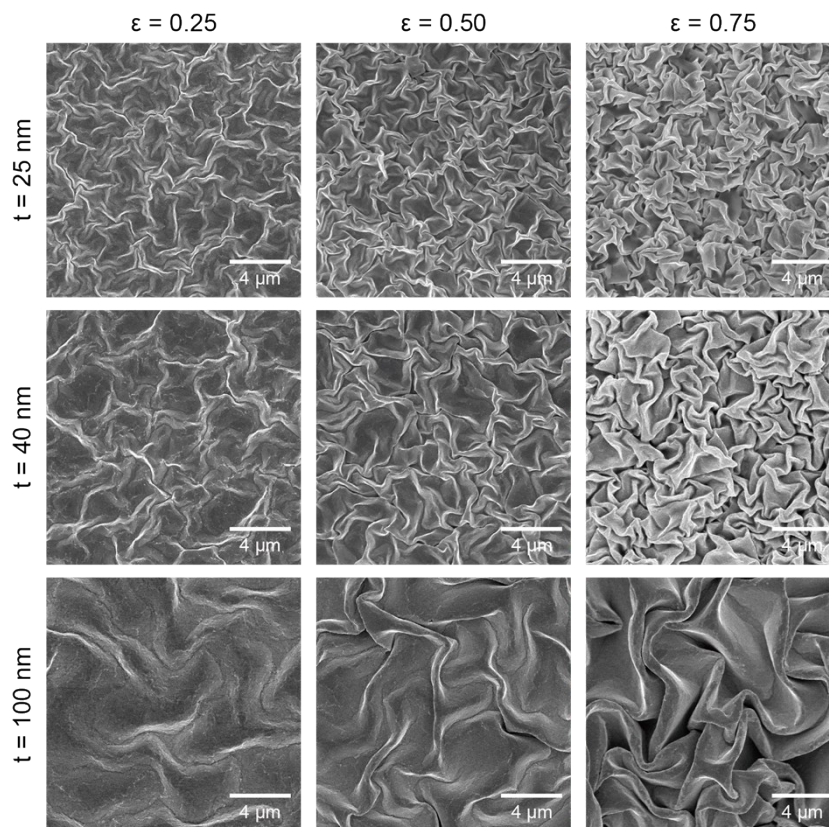

Figure S1. SEM images of wrinkles with varying thickness and strain.

CO$_2$RR test and morphology analysis of thickness-controlled c-wrinkle

The CO$_2$RR tests were conducted under the electrolyte of KHCO$_3$ (0.1 M and 0.5 M). The thickness of skin layer on c-wrinkle (ε=0.75) changed from 25 nm to 100 nm. The amplitude of c-wrinkle was 0.4 (ε=0.25), 0.7 (ε=0.5) and 2.2 μm (ε=0.75; Figure **S2b**).
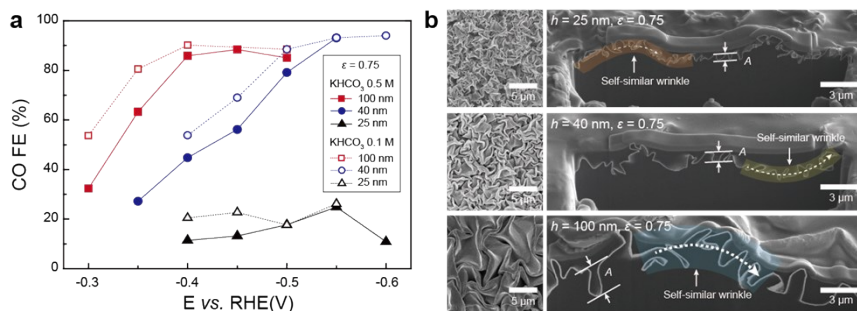

Figure S2. CO$_2$RR test and morphology analysis of thickness-controlled wrinkles. (a) The faradaic efficiency of CO and (b) Top-view and cross-sectional SEM images of Au wrinkles (t = 25 nm, 40 nm and 100 nm; ε = 0.75)

CO$_2$RR test using various electrolytes with different buffer strength

The CO$_2$RR tests were conducted under the electrolyte of KClO4 (0.1 M), KHCO$_3$ (0.1 M), and K$_2$HPO$_4$ (0.1 M). Compared to KHCO$_3$, KClO$_4$ has no buffering ability and K$_2$HPO$_4$ has strong buffering ability. Au wrinkle (ε=0.5 and ε=0.25) showed much difference in CO FE under KClO$_4$ and KHCO$_3$ because buffer effect of KHCO$_3$ suppress the CO formation. On the other hands, Au wrinkle (ε=0.75) showed very close CO FE between KClO$_4$ and KHCO$_3$ because its confined cavity creates a local pH. Indeed, Au wrinkle (ε=0.75) exhibited ~60% under the K$_2$HPO$_4$ having strong buffer strength. Accordingly, confined wrinkle has an effective morphology to create a local pH, leading selective CO formation.
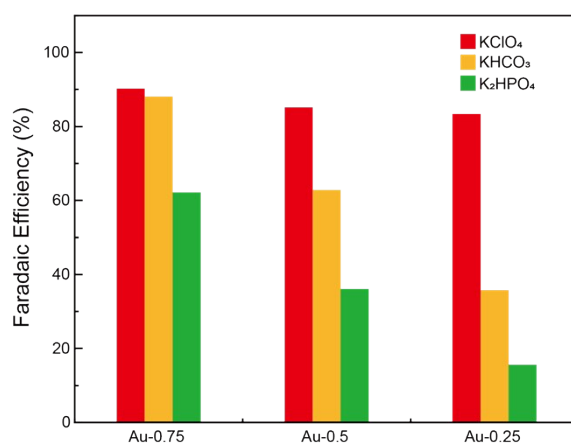

Figure S3. CO$_2$RR test under different electrolytes of KClO$_4$, KHCO$_3$ and K$_2$HPO$_4$.

The local pH effect of o-wrinkle depending on its amplitude

We controlled the amplitude of o-wrinkle with constant ε and t by using the sacrificial layer (PVP). When we controlled the concentration of PVP (from 2 to 8 wt%), the corresponding amplitudes were from 0.6 to 2.1 nm, respectively. The CO_2RR was conducted at -0.35 V vs. RHE under CO_2-saturated 0.5 M $KHCO_3$. It showed no much different activity of CO_2RR when the amplitude changed (FE_{CO} of ~10%)
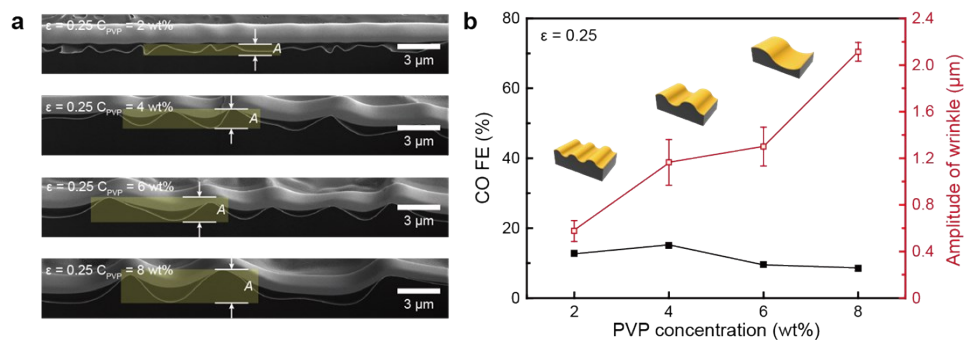
Figure S4. **CO_2RR performance for o-wrinkle with various amplitudes.** (a) cross-sectional SEM images and (b) faradaic efficiency of CO of o-wrinkle with different amplitudes.

Measurement of ECSA of Au wrinkle film

We measured ECSA of Au wrinkle films with a thickness of 25, 40 and 100 nm and strain of 0.5 and 0.75. ECSA was determined by adsorbed monolayer oxygen atom. The peak at ~0.85 V indicated reduction of adsorbed oxygen. The electrochemical surface area of wrinkle film (ε = 0.25, 0.5 and 0.75) is 1.5-times, 2.8-times and 4-times greater than flat film. Theoretically, without re-construction of surface morphology, the surface area would be increased to 1.33-times, 2-times and 4-times, in accordance with measured ECSA.
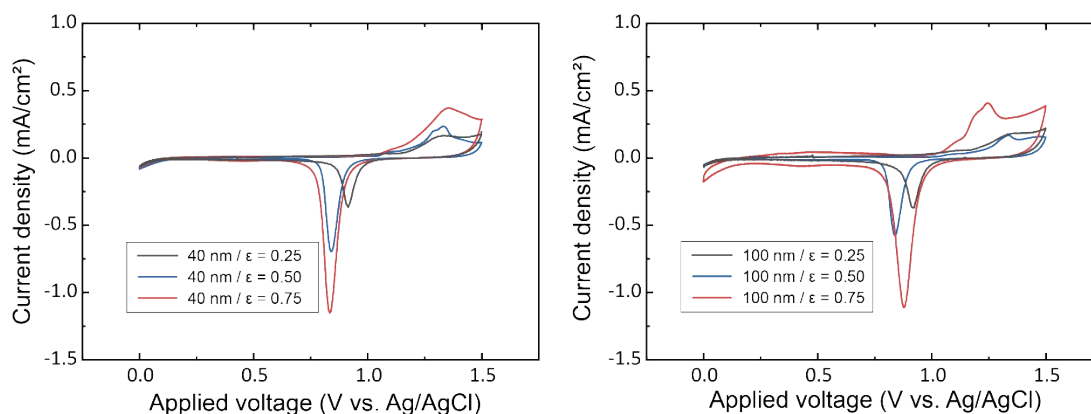
Figure S5. **The measurement of electrochemical surface area of Au wrinkles (t = 25, 40 and 100 nm, ε = 0.25, 0.5 to 0.75). The peaks of CV are indicative of adsorption and desorption of physisorption of oxygen atom.**

Investigation of surface facet of Au wrinkle using Pb underpotential deposition

The facet of Au was determined by Pb underpotential deposition, where the peaks at -0.49 V and -0.35 V indicative of (111) and (100) of Au facet. The facet shows no much difference between wrinkles at ε of 0.25 and 0.75.
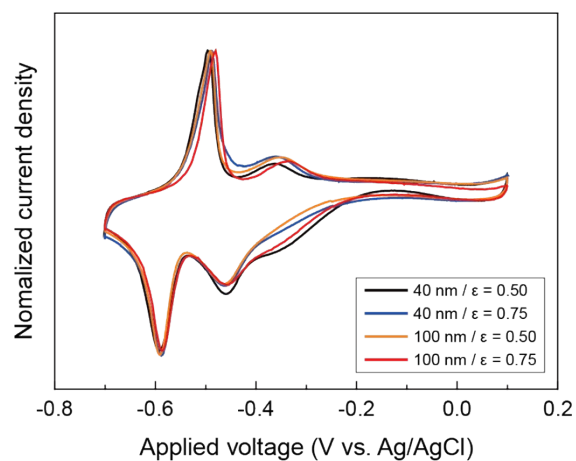

Figure S6. **The underpotential deposition of Pb on Au wrinkles (t = 40 and 100 nm, ε = 0.25 to 0.75)**

Cross-sectional SEM image of fully-opened wrinkle structure at a high strain

In the case of hierarchical wrinkles, the strain is divided into three parts. Because the confined wrinkles do not appear in the low strain range ($\varepsilon < 0.5$), if we create the wrinkles in three different wavelength ranges and create them in the low strain range, we can get a structure with the fully opened wrinkles as shown in **Figure S7**. This hierarchical wrinkle structure is made by using polyvinylpyrrolidone (PVP) as a sacrificial layer. When the skin layer is made by coating PVP on the first wrinkle, larger wrinkles are produced by applying the next strain. Next, coating a higher concentration of PVP solution and making a third wrinkle resulted in a wrinkle of fully opened structures with a larger wavelength. In this work, we used 0 wt%, 3 wt% and 10 wt% PVP solutions for first, second and third wrinkle structures with each $\varepsilon = 0.37$.
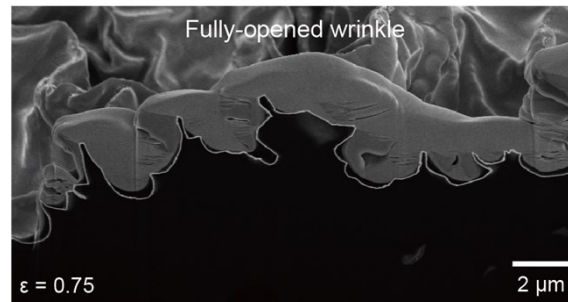

Figure S7. Cross-sectional SEM image of fully-opened wrinkle structure.

Concentration distribution from flow and diffusion effects

In the computational modeling of the spatiotemporal distribution of ion concentration, we consider two primary mechanisms for mass transport; (1) flow and (2) diffusion. To clarify the effects of flow and diffusion, we conducted coupled convection-diffusion simulation with COMSOL Multiphysics. The liquid flow from the stirring was modelled with the Laminar flow boundary condition because the distance between the boundary and the wrinkled geometry is significantly larger than the characteristic scale of the wrinkle, while the constant rate of OH-ion generation at the wrinkled geometry ($1.04 \times 10^{-4} mol/m \cdot s$) is assumed (**Figure S7a**). Our simulation reveals that the effect of the flow on the opened wrinkle structure is very small compared to the effect of diffusion and that the ion concentration is dominantly decided by the diffusional effect (**Figure S7b, c**). In the case of the confined wrinkle structure, no mass transport occurs in the wrinkle due to the flow. As a result, mass transport is dominated by diffusion in both cases, so the local pH must be determined by the shape of the wrinkles.
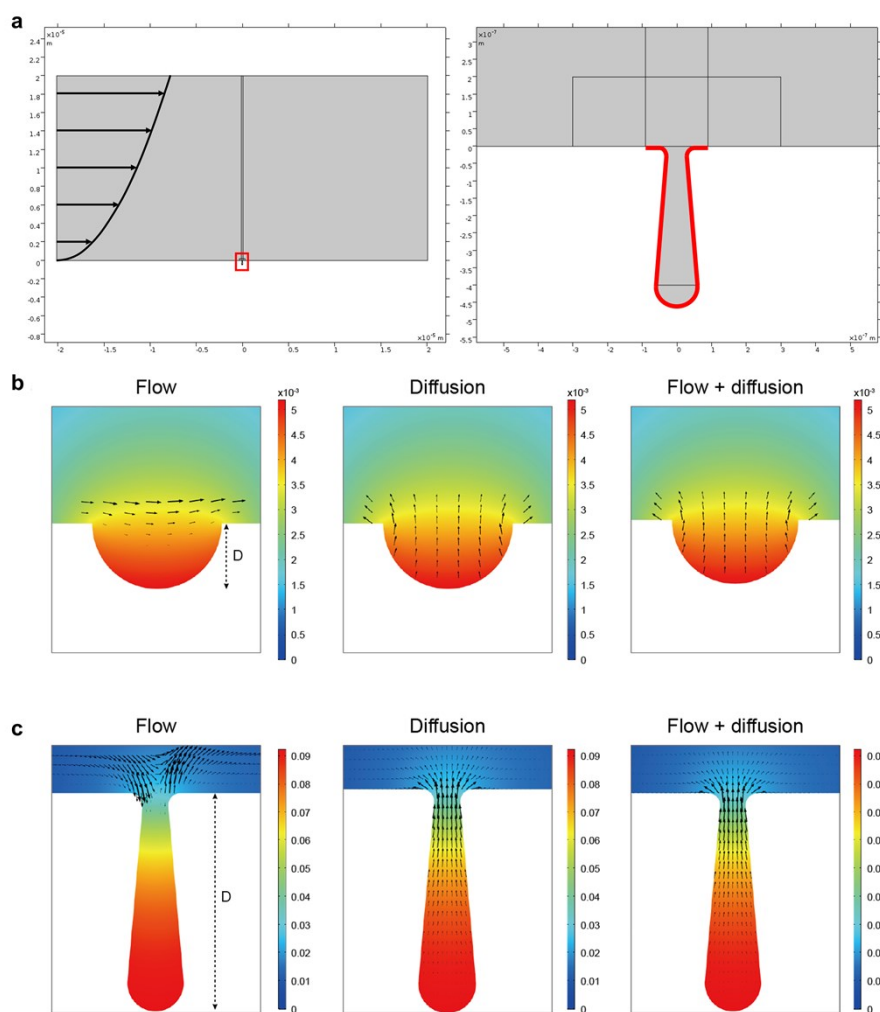
Figure S8. Concentration distribution from flow and diffusion effects. (a) Boundary condition for the simulation. The liquid flow from the stirring was modelled with the Laminar flow boundary condition because the distance between the boundary and the wrinkled geometry is significantly larger than the characteristic scale of the wrinkle, while the constant rate of OH- ion generation at the wrinkled geometry ($1.04 \times 10^{-4} mol/m \cdot s$) is assumed. (b, c) Simulation results of wrinkles with (b) $\varepsilon = 0.50$ and (c) $\varepsilon = 0.75$.

Synthesis of needle-like nanostructure on Au wrinkle

The nanostructure was fabricated on wrinkle films via electrodeposition method. The electrodeposition was conducted at -250 mV (*vs.* Ag/AgCl). At 150 s, the rod-like nanostructure was deposited. At 300 s, the needle-like structure was obtained. We conclude that the various nanostructure will be introduced onto the surface of wrinkle films.
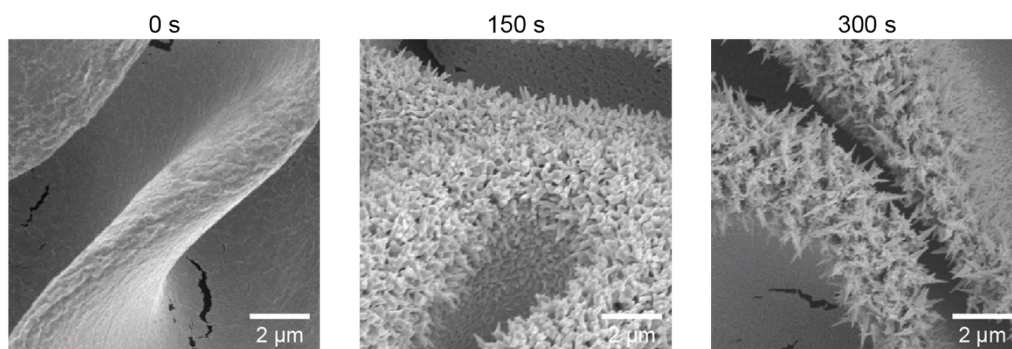

Figure S9. **Formation of nanostructured Au on the c-wrinkle by electrodeposition for 0 s, 150 s and 300 s.**